Supporting Information for:

Electron transfer within β-diketiminato nickel bromide and cobaltocene redox couples activating CO_2

Philipp Zimmermann, Alexander F. R. Kilpatrick, Deniz Ar, Serhiy Demeshko, Beatrice Cula, Christian Limberg*

Table of Contents

Experimental Section

General Considerations. All manipulations were carried out under an argon atmosphere using Schlenk techniques or in glove boxes under either dinitrogen or argon atmospheres maintained below 1 ppm of O_2 and H_2O. Glassware was heated under vacuum for approx. 10 min using a heat gun at 650 °C prior to use. Solvents were used purified from an MBraun solvent purification system (SPS). C_6D_6 was stored in a glove box and purified by 3 Å molecular sieves. IR spectra were recorded on a Bruker ALPHA spectrometer with an ATR sampling unit. EPR samples were recorded at a Bruker ESR 300 X-Band EPR or a X-band Bruker EMXplus spectroscope equipped with a recirculating Helium-cooling system ColdEdge-ER4112HV-CF10-H. Elemental analyses were performed with a HEKA Euro 3000 elemental analyzer. The magnetic data of the microcrystalline sample of **2** were recorded on a SQUID magnetometer (SQUID-VSM or MPMS3, Quantum Design) under an external magnetic field (0.5 T) in the temperature range of 2–300 K.

$L^{tBu}NiBr$[1] was prepared according to the literature procedure. Cp^*_2Co and Cp_2Co were purchased from Sigma Aldrich.

Synthesis of [L^{tBu}NiBr][$CoCp^*_2$], 1.

To a solution of L^{tBu}NiBr (82.3 mg, 0.13 mmol) in 2.5 mL toluene a solution of $CoCp^*_2$ (42.3 mg, 0.13 mmol, 1 eq.) in 2 mL toluene was added and the resulting brown solution shaken for one minute. After standing for 1 h the supernatant was filtered off and the resulting crystalline residue washed with hexane. After evaporation of all volatiles **1** was isolated as a bronze coloured crystalline solid (97.0 mg, 0.10 mmol) in 78 % yield.

ATR-IR (solid): ν = 2954, 2897. 2860, 2076, 1584, 1498, 1441, 1408, 1362, 1321, 1253, 1219, 1195, 1150, 1095, 1056, 1022, 963, 936, 879, 845, 799, 774, 764, 754, 700, 590, 532, 443 cm^{-1}.

Elemental analysis calc. (%) for $C_{55}H_{83}BrCoN_2Ni$ (969.79 $g*mol^{-1}$): C 68.12, H 8.63, N 2.89; found: C 67.36, H 8.44, N 2.91.

Crystals suitable for X-ray diffraction analysis were grown from a toluene solution at -30 °C.

Synthesis of [L^{tBu}NiBr][Cp_2Co], 2.

A solution of $CoCp_2$ (28.9 mg, 0.15 mmol, 1 eq.) in toluene (1 mL) was added to a solution of L^{tBu}NiBr (98.0 mg, 0.15 mmol) in toluene (2 mL) and the resulting red solution stirred for one minute. Subsequently, it was stored at room temperature. Within 3 hours a red crystalline precipitate formed, from which the supernatant was filtered off. The solid was washed with 0.2 mL of toluene, and after evaporation of all volatiles, **2** was isolated as a red brown solid (77.0 mg). After storing the mother liquor at -30 °C for 2 days, another crop of red crystalline solid could be obtained. Filtering off the supernatant and evaporation of all solvent gave another portion of **2** (38.9 mg; total yield: 115.9 mg, 91 %).

ATR-IR (solid): ν = 3097, 3040, 3010, 2955, 2901, 2863, 1582, 1524, 1498, 1461, 1444, 1407, 1362, 1322, 1279, 1252, 1218, 1196, 1151, 1095, 1057, 1029, 1002, 962, 935, 888, 860, 801, 775, 768, 756, 731, 696, 684, 647, 505, 465, 435, 407 cm^{-1}.

Elemental analysis calc. (%) for $C_{45}H_{63}BrCoN_2Ni$ (829.53 g*mol^{-1}): C 65.16, H 7.66, N 3.38; found: C 65.62, H 7.75, N 3.40.

Crystals suitable for X-ray diffraction analysis were grown from a Et_2O solution at -30 °C.

Colour changes observed for 2 upon variation of the temperature

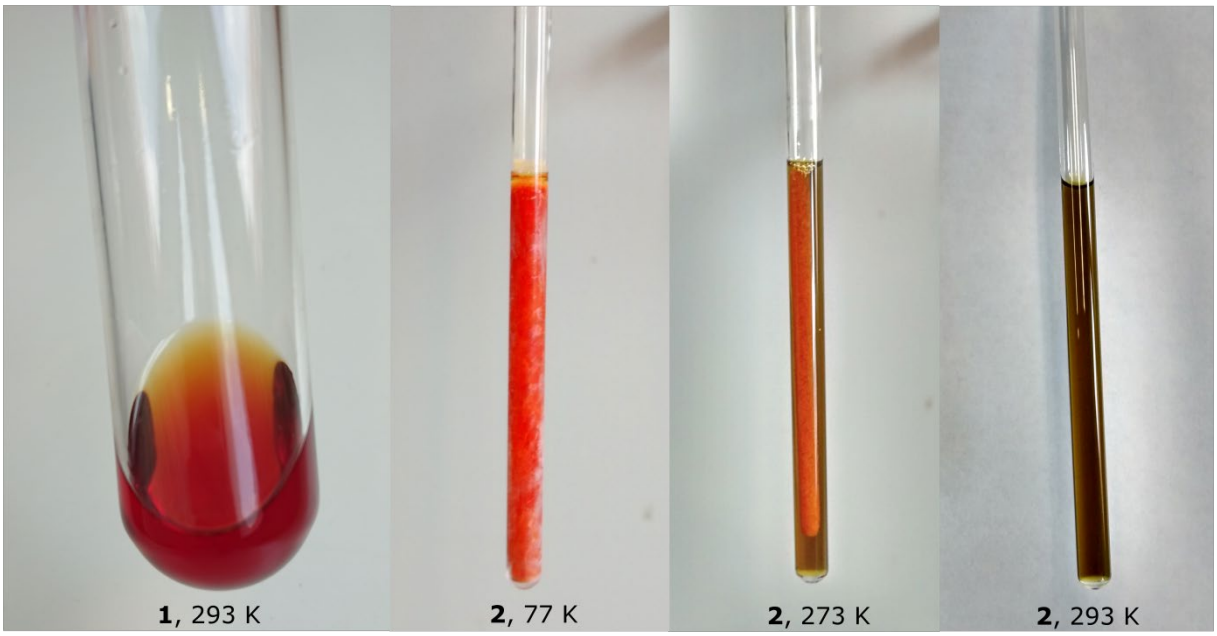

Figure S1. Colour of solution of **1** in toluene at ambient temperature and colour changes observed for solutions of **2** in C_6D_6 upon freezing/thawing.

Reaction of 1 with CO_2, generation of [L^{tBu}NiCO$_3$][CoCp*$_2$].

A solution of **1** (0.5 mg, 0.001 mmol) in C_6D_6 in an NMR tube sealed with a J. Young valve was degassed and the atmosphere exchanged with CO_2 gas. After shaking for 1 minute, the solution became cloudy. The resulting suspension was analysed by means of ATR-IR spectroscopy.

ATR-IR (solid): ν = 3060, 2960, 2926, 2868, 1710, 1620, 1518, 1461, 1433, 1408, 1366, 1320, 1259, 1220, 1181, 1093, 1015, 935, 865, 794, 763, 700, 636, 449 cm^{-1}.

Reaction of 1 with $^{13}CO_2$, generation of [L^{tBu}Ni(^{13}C)O$_3$][CoCp*$_2$].

A solution of **1** (0.5 mg, 0.001 mmol) in C_6D_6 in an NMR tube sealed with a J. Young valve was degassed and the atmosphere exchanged with $^{13}CO_2$ gas. After shaking for 1 minute the solution became cloudy. The resulting suspension was analysed by means of ATR-IR spectroscopy.

ATR-IR (solid): ν = 3312, 3060, 2959, 2920, 2852, 1633, 1619, 1588, 1536, 1516, 1459, 1428, 1408, 1383, 1365, 1321, 1260, 1220, 1179, 1163, 1096, 1017, 935, 865, 795, 762, 721, 685, 638, 585, 505, 449 cm^{-1}.

Synthesis of [$L^{tBu}NiCO_3$][$CoCp_2$], 3.

A solution of **2** (51.0 mg, 0.06 mmol) in toluene (6 mL) was degassed and the atmosphere was exchanged by CO_2. After standing for one week, the supernatant was filtered off and the crystalline residue dried under vacuum. After washing with Et_2O and evaporation of all volatiles, **3** was isolated as a brown solid (6.1 mg, 0.01 mmol, 25 % absolute yield, 50 % relative yield).

ATR-IR (solid): ν = 3062, 2960, 2927, 2868, 1710, 1619, 1588, 1564, 1534, 1518, 1461, 1431, 1408, 1382, 1362, 1323, 1259, 1219, 1178, 1103, 1058, 1043, 1018, 984, 957, 934, 862, 795, 761, 726, 684, 637, 583, 555, 518, 497, 463 cm^{-1}.

Elemental analysis calc. (%) for $C_{46}H_{63}CoN_2NiO_3$ (809.63 $g*mol^{-1}$): C 68.24, H 7.84, N 3.46; found: C 66.67, H 8.56, N 3.88. Crystals suitable for X-ray diffraction analysis were grown from a C_6D_6 solution.

Reaction of 2 with $^{13}CO_2$, generation of [$L^{tBu}Ni(^{13}C)O_3$][$CoCp_2$].

A solution of **2** (12.3 mg, 0.015 mmol) in C_6D_6 in an NMR tube sealed with a J. Young valve was degassed and the atmosphere exchanged with CO_2 gas. After 30 minutes the solution became cloudy and after 24 h a microcrystalline solid had precipitated. The resulting suspension was analysed by means of ATR-IR.

ATR-IR (solid): ν = 3063, 2961, 2868, 1618, 1587, 1578, 1518, 1462, 1430, 1411, 1393, 1382, 1363, 1322, 1260, 1229, 1178, 1161, 1105, 1058, 1043, 1012, 934, 861, 805, 794, 761, 727, 684, 637, 497, 465, 433, 408 cm^{-1}.

Electrochemistry

Electrochemical studies were carried out using a PalmSens EmStat Blue potentiostat under computer control. Cyclic voltammetry experiments were performed under argon using a three-electrode configuration with a glassy carbon disc (7.0 mm^2) as the working electrode, a Pt wire as the counter electrode and a Ag wire as the pseudo-reference electrode. Sample solutions were prepared by dissolving the analyte (*ca.* 5 mM) in THF (3.0 cm^3) followed by addition of a supporting electrolyte [^{n}Bu$_4$N][PF$_6$]. The reported mid-peak potentials are referenced internally to that of the $FeCp_2^{+/0}$ redox couple, which was measured by adding ferrocene (*ca*. 0.5 mg) to the sample solution.

Cyclic Voltammograms recorded in addition to those displayed in Figure 4

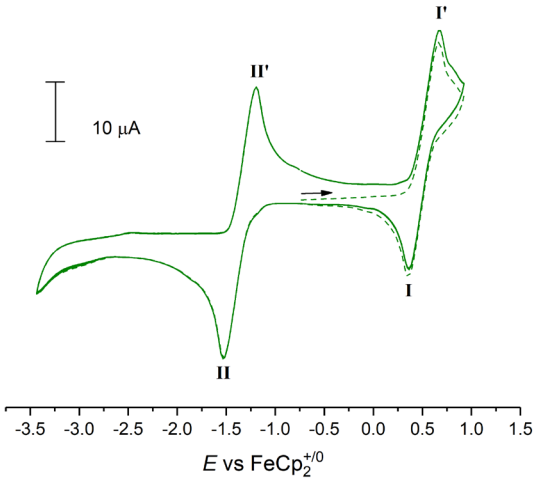

Figure S2. CV scans (4 cycles) of $^{t\text{Bu}}$LNiBr in THF/0.1 M [^{n}Bu$_4$N][PF$_6$], scan rate 100 mV s^{-1}. Dotted line denotes first scan.

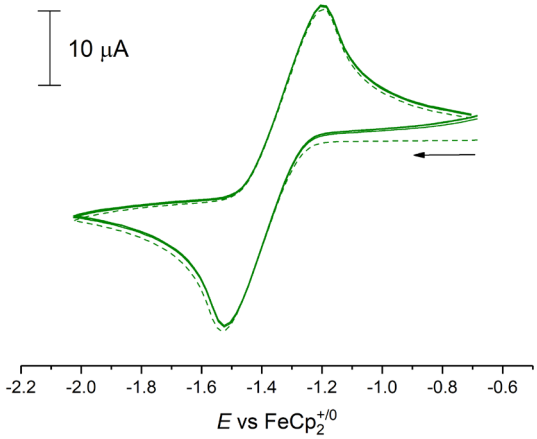

Figure S3. CV scans (4 cycles) of $^{t\text{Bu}}$LNiBr in THF/0.1 M [^{n}Bu$_4$N][PF$_6$], scan rate 100 mV s^{-1}. Dotted line denotes first scan.

Table S1. CV peak potentials (E_p vs $FeCp_2^{+/0}$) and limiting currents (i_p) for ^{tBu}LNiBr in THF / 0.1 M [^{n}Bu$_4$N][PF$_6$] at scan rate 100 mV s^{-1}.

	E_{pa} / V	E_{pc} / V	$E_{½}$ / V	ΔE_{pp} / mV	i_{pa} / µA	i_{pc} / µA	$\lvert i_{pa}/i_{pc} \rvert$
Process I	0.665	0.365	0.515	300	25.485	−17.720	1.44
Process II	−1.195	−1.535	−1.365	340	24.710	−25.369	0.97

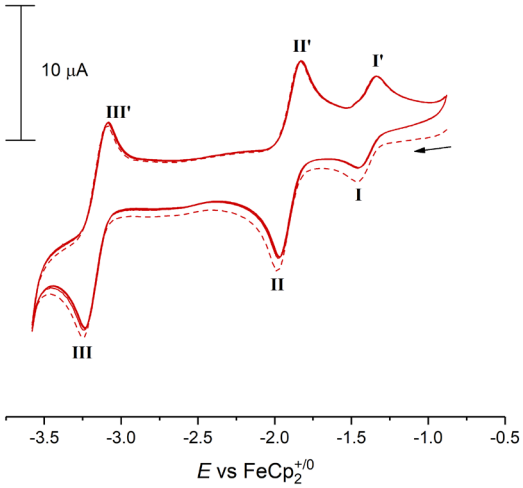

Figure S4. CV scans (4 cycles) of [^{tBu}LNiBr][CoCp*$_2$] in THF/0.1 M [^{n}Bu$_4$N][PF$_6$], scan rate 100 mV s^{-1}. Dotted line denotes first scan.

Table S2. CV peak potentials (E_p vs $FeCp_2^{+/0}$) and limiting currents (i_p) for [^{tBu}LNiBr][CoCp*$_2$] in THF / 0.1 M [^{n}Bu$_4$N][PF$_6$] at scan rate 100 mV s^{-1}.

	E_{pa} / V	E_{pc} / V	$E_{½}$ / V	ΔE_{pp} / mV	i_{pa} / µA	i_{pc} / µA	$\lvert i_{pa}/i_{pc} \rvert$
Process I	−1.34	−1.98	-1.66	0.64	2.365	−2.117	1.12
Process II	−1.82	−1.97	-1.90	0.15	6.509	−7.202	0.90
Process III	−3.23	−3.08	-3.155	−0.15	7.141	−8.784	0.81

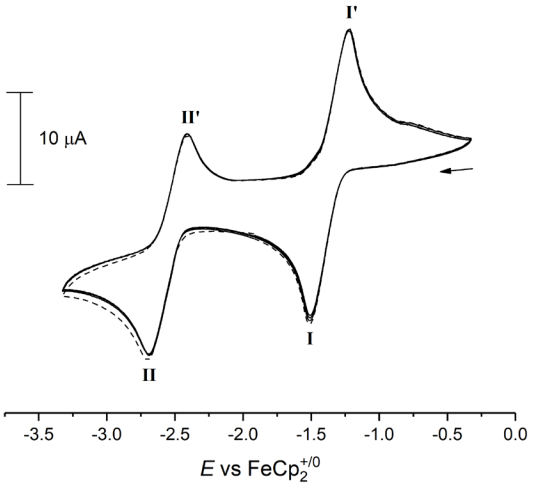

Figure S5. CV scans (4 cycles) of [^{tBu}LNiBr][$CoCp_2$] in THF/0.1 M [$^{n}Bu_4N$][PF_6], scan rate 100 mV s^{-1}. Dotted line denotes first scan.

Table S3. CV peak potentials (E_p vs $FeCp_2^{+/0}$) and limiting currents (i_p) for [^{tBu}LNiBr][$CoCp_2$] in THF / 0.1 M [$^{n}Bu_4N$][PF_6] at scan rate 100 mV s^{-1}.

	E_{pa} / V	E_{pc} / V	$E_{½}$ / V	ΔE_{pp} / mV	i_{pa} / μA	i_{pc} / μA	$\lvert i_{pa}/i_{pc} \rvert$
Process I	−1.225	−1.505	−1.365	0.28	14.20	−15.32	0.93
Process II	−2.415	−2.685	−2.55	0.27	11.61	−13.1	0.89

IR spectra

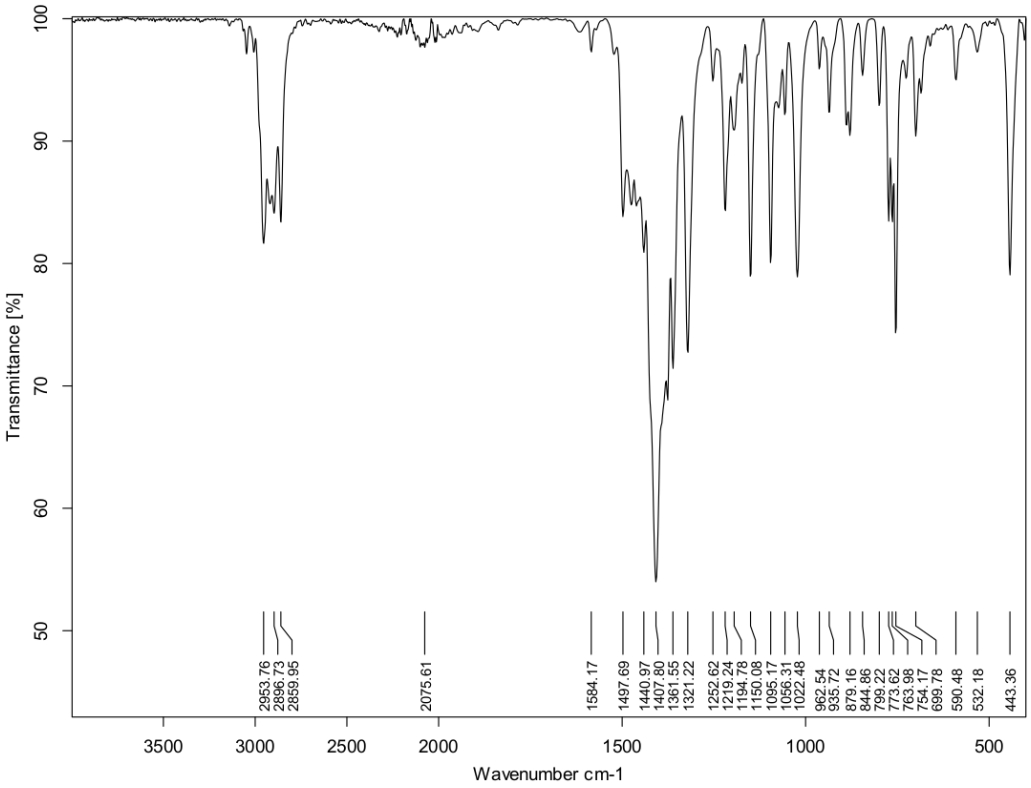

Figure S6. ATR-IR spectrum of (solid) **1**.

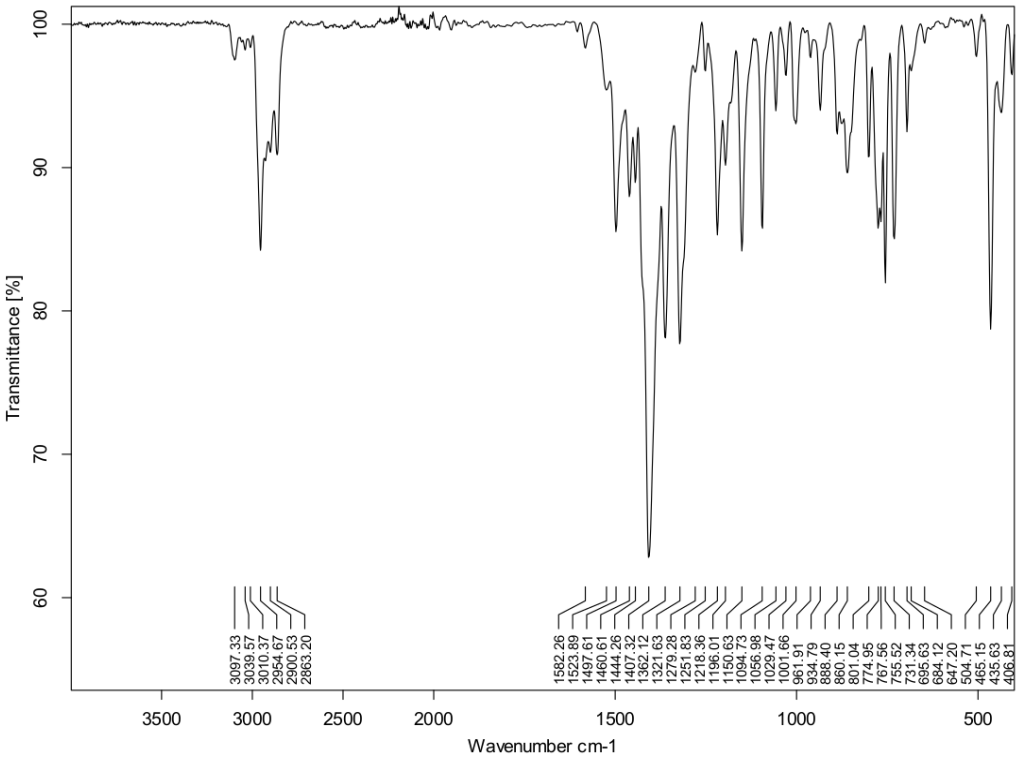

Figure S7. ATR-IR spectrum of (solid) **2**.

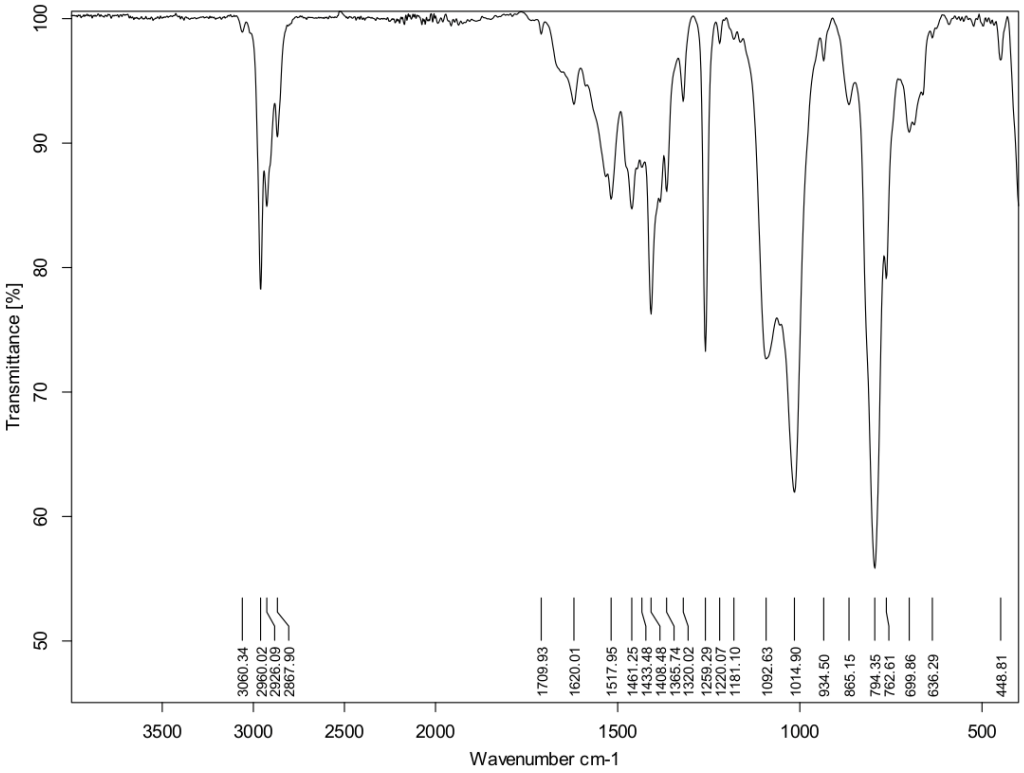

Figure S8. ATR-IR spectrum of the (solid) reaction mixture obtained after the reaction of **1** with CO_2 and evaporation of all volatiles.

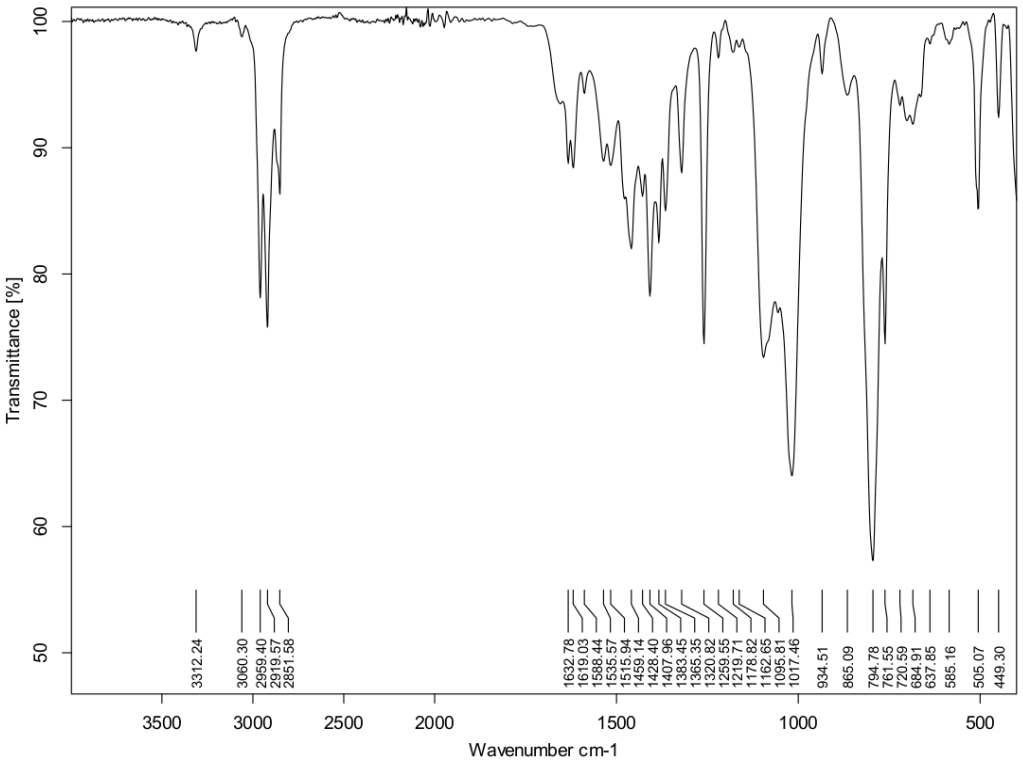

Figure S9. ATR-IR spectrum of the (solid) reaction mixture obtained after the reaction of **1** with $^{13}CO_2$ and evaporation of all volatiles.

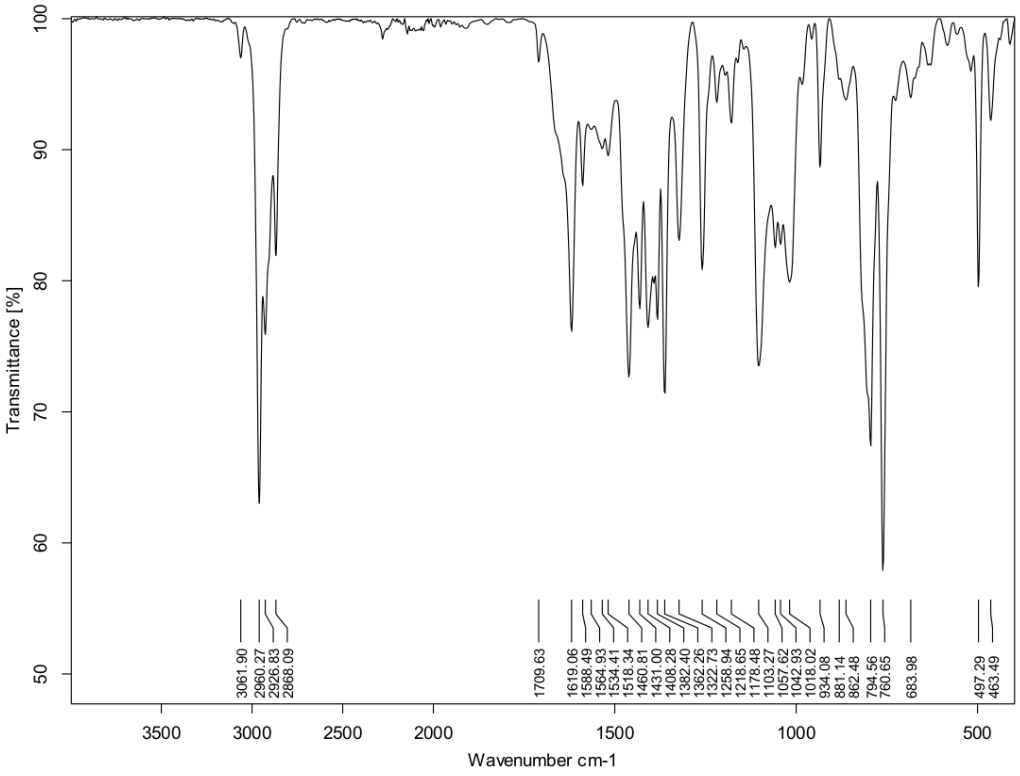

Figure S10. ATR-IR spectrum of (solid) **3**.

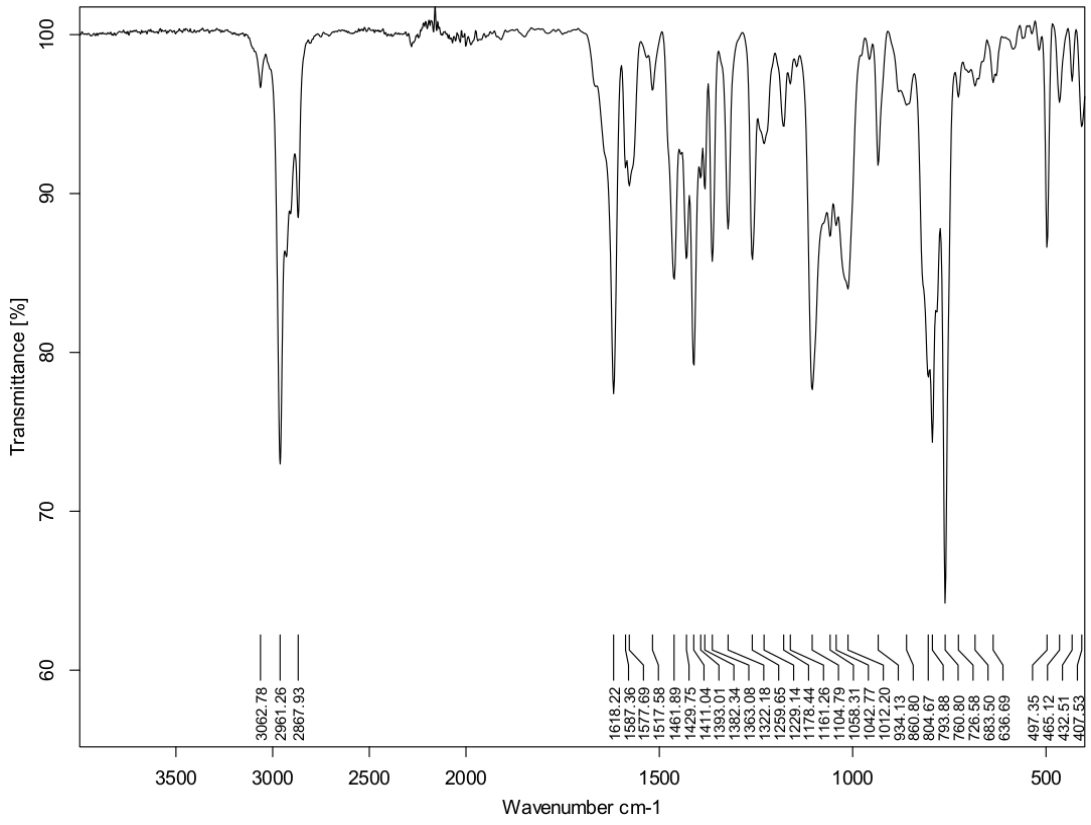

Figure S11. ATR-IR spectrum of the (solid) reaction mixture obtained after the reaction of **2** with $^{13}CO_2$ and evaporation of all volatiles.

EPR spectra

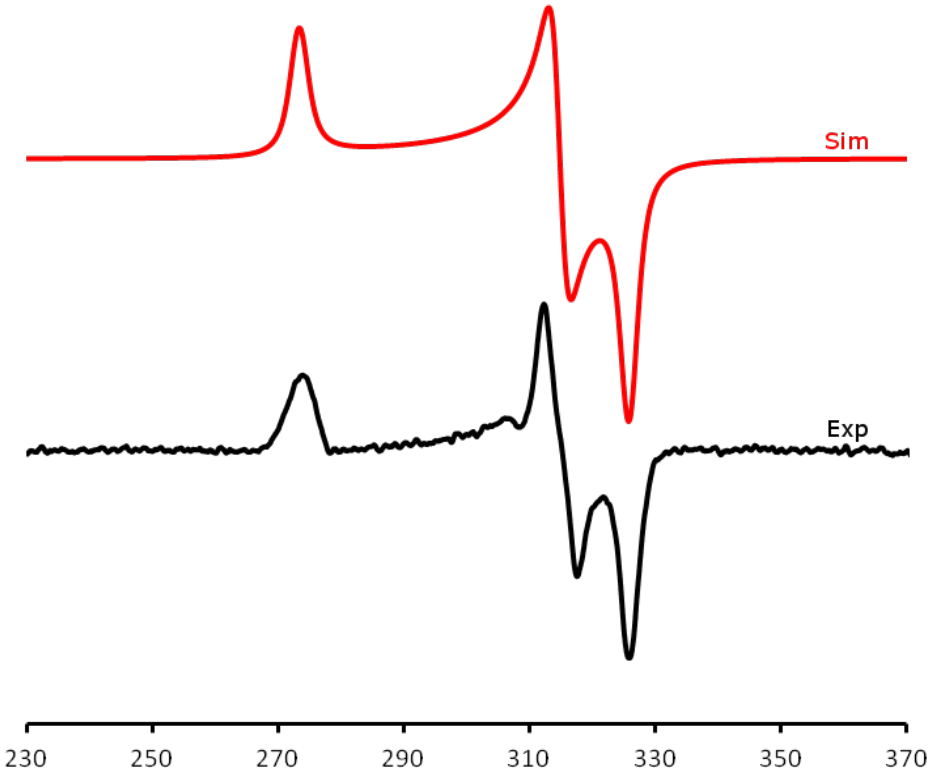

Figure S12. X-band EPR spectrum of a solid sample of **1** (black) at 77 K and powder simulation (red) with g_1 = 2.469, g_2 = 2.144, and g_3 = 2.071.

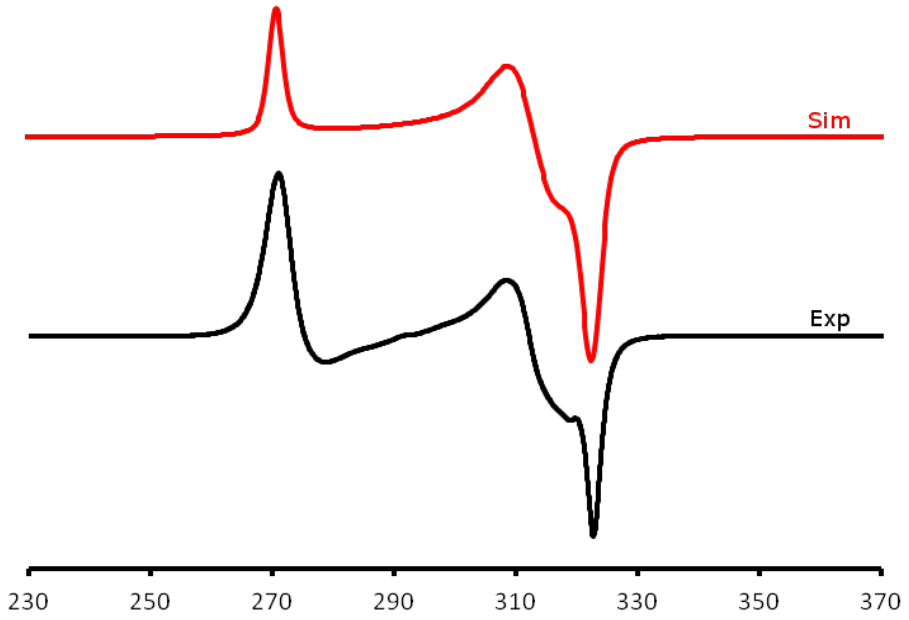

Figure S13. X-band EPR spectrum of a solid sample of **2** (black) at 13 K and powder simulation (red) with g_1 = 2.466, g_2 =2.136, and g_3 = 2.072.

Calculation of thermodynamic data for the dissociation of **2** from variable temperature EPR spectroscopy, quantified utilizing a TEMPOL (4-Hydroxy-TEMPO) (1.0 mmol·L^{-1} in toluene) standard.

Dissociation of **2** to L^{tBu}NiBr and Cp_2Co**:**

$[L^{tBu}Ni^{I}Br][Cp_2Co^{III}] \rightleftharpoons L^{tBu}Ni^{II}Br + Cp_2Co^{II}$

$$K = \frac{c(Ni^{II})^2}{c(Ni^{I})}$$

$$c_0(Ni^{I}) = 1.324\ \text{mmol} \cdot L^{-1}$$

$$c(Ni^{II}) = c_0(Ni^{I}) - c(Ni^{I})$$

$$c(Ni^{I}) = c_0(Ni^{I}) \cdot \frac{Yield(Ni^{I})}{100}$$

Table S1. Determination of the equilibrium constants (K) for dissociation of **2** at different temperatures.

T / K	T^{-1} / K^{-1}	Yield Ni^{I} EPR Signal in %	c(Ni^{I}) / mmol·L^{-1}	c(Ni^{II}) / mmol·L^{-1}	K	ln K
293		0				
273	0.003663	4.15	0.054946	1.269054	0.0341174	– 3.377948
253	0.003952	7.70	0.101948	1.222052	0.0682652	– 2.684355
233	0.004292	17.77	0.235274	1.088725	0.1984901	– 1.617016
183	0.005464	59.88	0.792811	0.531188	2.8097776	1.033105

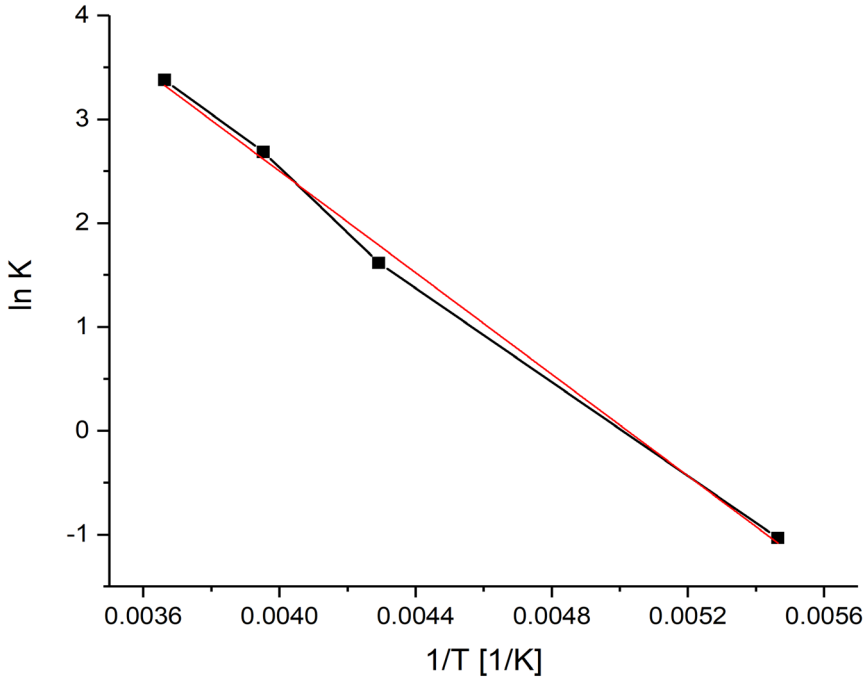

Figure S14. Van't Hoff plot (R^2 = 0.9966) of ln K vs. T^{-1} for determination of thermodynamic data for the dissociation of **2**.

$$\ln K_{eq} = \Delta H \frac{1}{RT} + \Delta S \frac{1}{R}$$ Van't Hoff plot

$$\Delta H = \text{Slope} \cdot R$$

$$\Delta S = \text{Intercept} \cdot R$$

Table S2. Considerations for determination of thermodynamic data for dissociation of **2** from the Van't Hoff plot.

		STD
Slope	2446	101.4
Intercept	– 12.28	0.4458
Gas constant R / J·mol^{-1}	8.314551	

Table S3. Thermodynamic data for dissociation of **2**, obtained from the Van't Hoff plot.

	H / kJ·mol^{-1}	**S / J·mol^{-1}**
	– 20.33739175	– 102.10269
STD	0.843095471	3.70662684

SQUID magnetometry

Temperature-dependent magnetic susceptibility measurements were carried out with a *Quantum-Design* MPMS3 SQUID magnetometer equipped with a 7 Tesla magnet in the range from 295 to 2.0 K at a magnetic field of 0.5 T. The powdered sample was contained in a polycarbonate capsule and fixed in a non-magnetic sample holder. Each raw data file for the measured magnetic moment was corrected for the diamagnetic contribution of the sample holder and the polycarbonate capsule. The molar susceptibility data were corrected for the diamagnetic contribution.

Simulation of the experimental magnetic data was performed with the *julX* program: E. Bill, Max-Planck Institute for Chemical Energy Conversion, Mülheim/Ruhr, Germany.

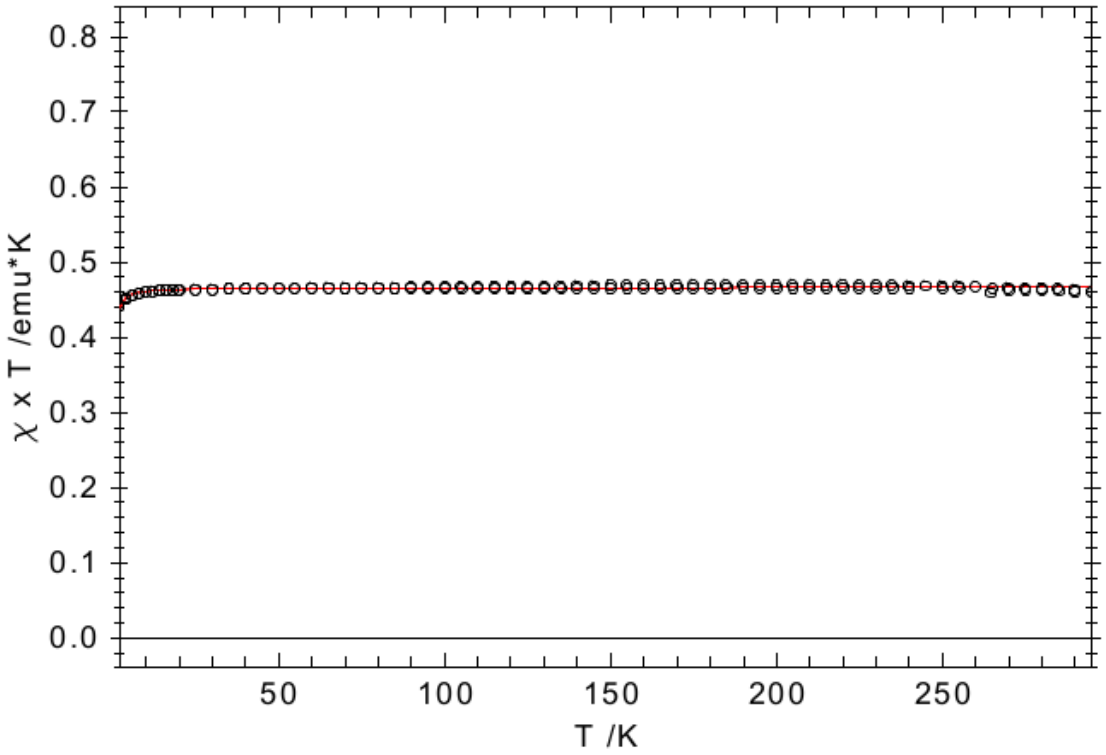

Figure S15. Plot (open circles) of χ_M*T against T for solid **2**. The red curve represents the best fit with parameters g = 2.23 (for S = ½), TIP = 650*10^{-6} cm^3mol^{-1} and θ (Weiss temperature) = –0.1 K.

X-Ray crystallographic information

The data collections were performed with a BRUKER D8 VENTURE area detector with Mo-Kα radiation (λ = 0.71073 Å). Multi-scan absorption corrections implemented in SADABS[2] were applied to the data. The structures were solved by intrinsic phasing method[3] and refined by full matrix least square procedures based on F^2 with all measured reflections[4] with anisotropic temperature factors for all non-hydrogen atoms. All hydrogen atoms were added geometrically and refined by using a riding model. Squeeze[5] refinement have been applied to the data of complex **2**.
CCDC numbers 2023971 (complex **1x3tol**), 2024643 (complex **2**) and 2023970 (complex **4**) contain the supplementary crystallographic data for this paper. These data can be obtained free of charge from The Cambridge Crystallographic Data Centre via www.ccdc.cam.ac.uk/data_request/cif.

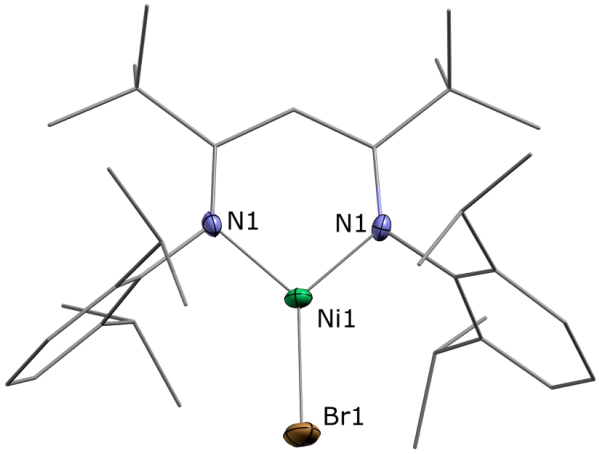

Figure S16. Molecular structure of L^{tBu}NiBr. Hydrogen atoms are omitted for clarity. Selected bond lengths /Å and angles /°: N1-Ni1 1.8112(16), Ni1-Br1 2.2781(5); N1-Ni1-Br1 131.81(13).

References

[1] S. Pfirrmann, C. Limberg, C. Herwig, R. Stößer, B. Ziemer, *Angew. Chem. Int. Ed.* **2009**, *48*, 3357-3361.
[2] G. M. Sheldrick, *SADABS* **1996**, University of Göttingen, Germany.
[3] G. M. Sheldrick, *Acta Crystallogr. A* **2015**, *71*, 3.
[4] G. M. Sheldrick, *Acta Crystallogr. C* **2015**, *71*, 3.
[5] A. L. Spek, *Acta Crystallogr. D, Biological crystallography* **2009**, *65*, 148.